Modelling the effect of nuclear motion on the attosecond time-resolved photoelectron spectra of ethylene

A Crawford-Uranga[1,*]**, U De Giovannini**[1]**, D J Mowbray**[1]**, S Kurth**[1,2]**and A Rubio**[1,*]

[1] Nano-Bio Spectroscopy Group and ETSF Scientific Development Center, Departamento de Física de Materiales, Centro de Física de Materiales CSIC-UPV/EHU-MPC and DIPC, Universidad del País Vasco UPV/EHU, Avenida de Tolosa 72, E-20018, San Sebastián, Spain
[2] IKERBASQUE, Basque Foundation for Science, E-48011, Bilbao, Spain

E-mail: `alisonc1986@gmail.com`, `angel.rubio@ehu.es`

Abstract
Using time dependent density functional theory (TDDFT) we examine the energy, angular and time-resolved photoelectron spectra (TRPES) of ethylene in a pump-probe setup. To simulate TRPES we expose ethylene to an ultraviolet (UV) femtosecond pump pulse, followed by a time delayed extreme ultraviolet (XUV) probe pulse. Studying the photoemission spectra as a function of this delay provides us direct access to the dynamic evolution of the molecule's electronic levels. Further, by including the nuclei's motion, we provide direct chemical insight into the chemical reactivity of ethylene. These results show how angular and energy resolved TRPES could be used to directly probe electron and nucleus dynamics in molecules.
Keywords: attosecond pump probe, nuclear motion, TRPES, TDDFT
(Some figures may appear in colour only in the online journal)

1. Introduction

Time-resolved photoelectron spectroscopy (TRPES) is a well established technique for characterizing the electronic and nuclear dynamics occurring after photoabsorption in molecules [1–9]. It allows one to map the occupied electronic states of a given interacting system and complements the information one can gather from optical spectroscopy. TRPES is particularly suited to the study of ultrafast non-adiabatic processes because photoelectron spectroscopy is sensitive to both electronic configurations and nuclear dynamics.

Many open questions remain, linked to how composite electron-nucleus excitations or shake-up processes appear in time-resolved spectroscopies [10]. Much work has been done in solid state physics concerning phonon side-bands in photoelectron spectra [11, 12], and in molecular systems using both standard optical spectroscopies and time resolved transient absorption spectroscopy [13, 14]. With the advent of attosecond laser pulse technology [15, 16], its increased temporal resolution has allowed the direct observation and control of coherent electronic motion [17–19].

In TRPES experiments, a time-delayed probe laser photo-ionizes an electron out to an evolving (usually laser-generated) excited state. The outgoing electron's kinetic energy and angular distribution is then measured as a function of time [20].

The time-resolved photoelectron angular distribution (TRPAD), is frequently available in gas

*Authors to whom any correspondence should be addressed.

phase experiments. However, it is rarely analysed, since it is so difficult to interpret. This is because the random orientation of molecules in free space significantly broadens the results, and it is also complicated to observe the ejection dynamics in the molecular frame. For this reason, molecular pre-alignment [21] and coincidence techniques [22], have proven necessary to extract molecular properties from TRPADs. Even in the molecular frame, a quantitative analysis is a formidable task. This is due to factors such as the multi-electron nature of the system, the subtle coupling between nuclear and electronic degrees of freedom, and nonlinearities due to the relatively high laser intensities required.

To complement these advanced experimental techniques, accurate and robust theoretical methodologies are necessary for their clear interpretation [23]. However, the choice of which level of theory to use is often a difficult task.

On the one side, the direct solution of the full time-dependent Schrödinger equation for interacting electrons should provide a full description. However, in the presence of time-dependent external fields, the full solution is feasible only for two electrons in three dimensions [24–26]. On the other side, the single active electron approximation [27], often invoked in many theoretical works, is likely to break down for large molecules. This has been indicated by recent experiments in the strong field regime [28].

Several approaches have been employed to model TRPES and TRPAD experiments on molecular systems. These include methods based on Hartree-Fock theory coupled to the Schwinger equation [29, 30]; schemes involving the projection onto states calculated with static density functional theory [31] or multi-scale second order perturbation theory with the ab initio multiple spawning method [32, 33]; the Wigner distribution approach with on-the-fly dynamics [34], and partitioning techniques applied to coupled equation schemes [35]. Most of these methods evaluate matrix elements involving continuum states, which are difficult to describe.

Time-dependent density functional theory (TDDFT) [36, 37] combined with a space partitioning scheme provides an attractive alternative. This is because this method does not require an explicit evaluation of continuum states. The sampling-point method has been successfully used to study the PES of small clusters [38, 39]. However, this method has suffered from numeri-

cal limitations in both angular resolution and total pulse length. The recently introduced mask-method [40], provides both better performance and full momentum resolution. Furthermore, it is non-perturbative and includes any interference between different ionization channels. It is this method which we employ in the present paper.

Previously we demonstrated how TDDFT can be used to describe time-resolved spectroscopies [41]. In principle, this allows one to handle large scale systems at a reasonable computational cost. However, we only considered the electronic degrees of freedom without analysing the impact of nuclear vibrations.

In the present work we extend the previous theoretical TDDFT framework by including classical molecular dynamics (MD) through an Ehrenfest approach [42, 43]. We illustrate the combined framework for the case study of ethylene already studied in the literature [32, 33]. In particular, we investigate the effect of the nuclear degrees of freedom on the time evolution of the electronic $\pi \rightarrow \pi^*$ transition.

2. Methodology

Within TDDFT all physical properties of a system can be determined by knowing their functional dependence with respect to the interacting many-body density [44]. The crucial idea of both DFT and TDDFT, is to obtain this many-body density through a mapping from the density of a fictitious, auxiliary system of non-interacting electrons. The latter is the so-called Kohn-Sham (KS) system [45].

First, the ground state density is obtained by solving the KS equations self-consistently at the DFT level. The evolution of the system then follows according to the Time Dependent Kohn Sham (TDKS) equations (in atomic units):

$$i\frac{\partial \varphi_i(\mathbf{r}, t)}{\partial t} = \left(-\frac{1}{2}\nabla^2 + V_{KS}[n](\mathbf{r}, t)\right)\varphi_i(\mathbf{r}, t), \quad (1)$$

for $i = 1, \ldots, N/2$, where

$$n(\mathbf{r}, t) = \sum_{i=1}^{N/2} 2|\varphi_i(\mathbf{r}, t)|^2. \quad (2)$$

Here we assume an even number of electrons N, and a spin-restricted configuration in which all the KS spatial orbitals φ_i are doubly occupied. The

non-interacting electrons move in the KS potential V_{KS} defined as:

$$V_{KS}[n](\mathbf{r},t) = V_{las}(\mathbf{r},t) + V_{ne}(\mathbf{r},t)$$
$$+ \int d\mathbf{r}\, \frac{n(\mathbf{r}',t)}{|r-r'|} + V_{xc}[n](\mathbf{r},t), \qquad (3)$$

where $V_{las}(\mathbf{r},t) = \mathbf{r}\cdot\mathbf{E}(t) - \sum_j \mathbf{R}_j(t)\cdot\mathbf{E}(t)$ is the potential describing the pump and probe laser fields where $\mathbf{E}(t)$ is the electric field associated to the laser, $V_{ne}(\mathbf{r},t)$ is the electron-nucleus potential, the third term is the Hartree potential and $V_{xc}[n](\mathbf{r},t)$ is the exchange and correlation potential. However, the exact form for the exchange and correlation potential is generally unknown.

The electron-nucleus potential, for a system composed of M atoms, is given by:

$$V_{ne}(\mathbf{r},t) = -\sum_{j=1}^{M} \frac{Z_j}{|\mathbf{R}_j(t)-\mathbf{r}|}, \qquad (4)$$

where $\mathbf{R}_j(t) = \{\mathbf{R}_1(t),\ldots,\mathbf{R}_M(t)\}$ are the set of classical nucleus positions and Z_j are their respective charges. The electronic density depends parametrically on the nuclei's positions $\mathbf{R}_j(t)$. The motion of the nuclei is in turn determined by the electronic density gradient through Newton's equations of motion. The motion of nucleus j, with mass M_j, evolves according to the following dynamic equation:

$$M_j \frac{d^2\mathbf{R}_j(t)}{dt^2} = \int d\mathbf{r}\, n(\mathbf{r},t)\nabla_j[V_{ne}(\mathbf{r},t) + V_{las}(\mathbf{r},t)]$$
$$+ \nabla_j \sum_{\ell \neq j} \frac{Z_\ell Z_j}{|\mathbf{R}_j(t)-\mathbf{R}_\ell(t)|} \;. \qquad (5)$$

The Ehrenfest MD scheme consists of the time propagation of the coupled equations (1) and (5).

Photoelectrons are obtained using a space partitioning scheme [40]. At each time step, every KS orbital $\varphi_i(\mathbf{r},t) = \varphi_i^A(\mathbf{r},t) + \varphi_i^B(\mathbf{r},t)$ is divided into the part residing in an inner interaction region A, $\varphi_i^A(\mathbf{r},t)$, and the remainder $\varphi_i^B(\mathbf{r},t)$ in the complementary ionization region B. In region A we solve the coupled TDKS plus classical nuclear motion equations in the presence of a mask boundary absorber of a given width R_{ab}. Absorbed electrons are collected and evolved in momentum space as free Volkov states $\tilde{\varphi}_i^B(\mathbf{p},t)$ within the ionization region B. The boundary between A and B has to be placed at sufficiently large distances so that $\tilde{\varphi}_i^B(\mathbf{p},t)$ is composed of outgoing waves only. The momentum-resolved photoelectron probability is then

$$P(\mathbf{p}) = \lim_{t\to\infty} \sum_{i=1}^{N/2} 2|\tilde{\varphi}_i^B(\mathbf{p},t)|^2. \qquad (6)$$

Observables such as PES $P(E)$ or PAD $P(E,\theta,\phi)$ are obtained from $P(\mathbf{p})$ by integration or slicing respectively.

The exchange and correlation functional we use in this work is the well known local density approximation (LDA) coupled with an average-density self interaction correction (ADSIC) [46, 47] for the ground state and its adiabatic extension for TDDFT. The choice of ADSIC is motivated by its correct asymptotic behaviour in the ground state. In other words, for a large distance r from the molecule, $V_{xc} \sim -1/r$. The high-lying unoccupied KS bound states close to the ionization threshold are thus described more accurately than with an exponentially decaying xc potential. For ethylene, using LDA alone gives an unbound π_z^* state. This makes the $\pi_z \to \pi_z^*$ transition inaccesible with most standard xc-functionals. On the other hand, the combination of LDA and ADSIC has been successfully employed in conditions similar to the ones described in this work [48, 49].

In addition, we freeze the $1s$ electrons of the carbon cores into a pseudopotential generated within the Troullier-Martins scheme [50] as distributed in the OCTOPUS code. In this way we "dress" the carbon nucleus. As these core levels are strongly bound (~ 10.29 Ha for carbon) we expect that neither the pump nor the probe will ionize them.

The TDKS equations are discretized and solved using a finite differences method within the OCTOPUS code [51–53]. We employ a spherical grid of radius $R = 30\ a_0$ with a grid spacing of $\Delta R = 0.3\ a_0$. We introduce a $10\ a_0$ wide mask boundary absorber to collect the photoelectrons and prevent electronic reflections [40, 41]. A velocity Verlet algorithm is employed to propagate Newton's equations (5) and an enforced time-reversal symmetry operator [54] is used to time-step the TDKS equations, with a time step of $\Delta t = 1.2$ as. This is small enough to steadily propagate nuclear and electronic degrees of freedom in all the presented calculations.

The molecular geometry obtained by force minimization ($\leq 2.4 \times 10^{-5}\ \frac{\text{Ha}}{a_0}$) has the two carbon atoms placed on the x-axis at $x = \pm 1.169\ a_0$ and hydrogens in the xy-plane at $(x,y) = (\pm 2.120, \pm 1.785)\ a_0$. The carbon-carbon (C–C) bond-length of $2.337\ a_0$ is in fair agreement with the experimental one of $2.531\ a_0$ [55].
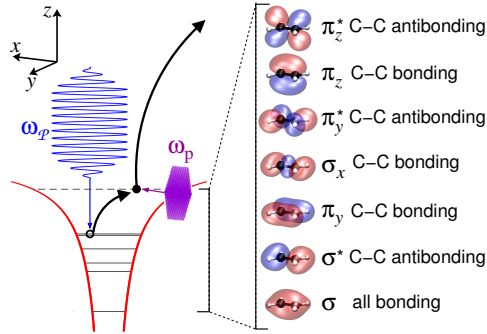
Figure 1. Schematic of the pump-probe setup employed to study the TRPES of ethylene. The pump (blue) is an ultraviolet (UV) laser pulse of energy $\omega_{\mathcal{P}} = 0.326$ Ha, with a 15 cycle trapezoidal shape (3 cycle ramp), and an intensity $I = 1.67 \times 10^{11}$ W/cm^2. polarized along the C–C bond, i.e., x axis. The excited electron is probed using an extreme ultraviolet (XUV) probe laser (violet) of energy $\omega_p = 1.8$ Ha, with a 40 cycle trapezoidal shape (8 cycle ramp), and an intensity of $I = 1.02 \times 10^{11}$ W/cm^2 polarized along the z axis. The calculated Hartree potential (red), KS eigenvalues (black horizontal lines), structural schematics (C in black, H in white), and KS orbitals (isosurfaces of $\pm 0.05 e/a_0^{3/2}$) for ethylene are shown according to their energy.

Moreover the first ionization potential obtained from LDA+ADSIC is $I_p = 0.447$ a_0, in agreement with the experimental value of 0.386 a_0 [56]. Here, I_p has been evaluated within DFT using the vacuum energy minus that of the highest occupied KS orbital, i.e., $I_p \approx E_{vac} - \varepsilon_{\text{HOMO}}$.

The photoionization process we consider is depicted schematically in figure 1, where the laser parameters have been adapted from Ref. [41]. A pump pulse resonantly populates the bound π_z^* state and the build-up is monitored at different times with a delayed probe laser. This is accomplished by applying an ultraviolet (UV) pump that is tuned to excite from the highest occupied molecular orbital (HOMO) to the lowest unoccupied molecular orbital (LUMO). For ethylene, this corresponds to a $\pi_z \rightarrow \pi_z^*$ transition.

In particular, we employ an UV pump laser of energy $\omega_{\mathcal{P}} = 0.326$ Ha, with a 15 cycle trapezoidal shape (3 cycle ramp), and an intensity $I = 1.67 \times 10^{11}$ W/cm^2 polarized along the x-axis. The probe is an XUV laser of energy $\omega_p = 1.8$ Ha, with a 40 cycle trapezoidal shape (8 cycle ramp), and an intensity of $I = 1.02 \times 10^{11}$ W/cm^2 polarized along the z-axis.

The time delay between the pump and the probe is measured from the onset of the pump probe is measured from the onset of the pump to the center of the probe so that negative delays correspond to cases where the probe precedes the pump. Moreover, we record photoelectrons only during the on-time of the probe pulse.

When we calculate the spectra for classically moving nuclei, we introduce an initial temperature of 300 K under the same pump-probe conditions. In this way, we may assess the impact of the nuclear degrees of freedom on the TRPES. The temperature is introduced in our model by assigning to each nucleus a random initial velocity consistent with a Boltzmann distribution at that temperature.

3. Results and Discussion

The TRPES for ethylene with the nuclei frozen at their equilibrium positions is shown in figure 2 (a). The spectra presents similar features to those described in Ref. [41].

The peak at $E_1 = 2\omega_{\mathcal{P}} - I_p = 0.205$ Ha constitutes the main ionization channel and it is due to the pump alone. Here, the absorption of a pump photon leading to a $\pi_z \rightarrow \pi_z^*$ transition, is followed by a second pump photon which directly excites electrons from the π_z^* state into the continuum. Multi-photon replicas of this peak can be observed at energies separated by integer multiples of $\omega_{\mathcal{P}}$.

The peak at $E_2 = \omega_p - I_p = 1.353$ Ha corresponds to the direct emission from the highest occupied KS orbital into the continuum.

A similar mechanism, but with electrons ejected from deeper levels, is responsible for the peaks lying at energies lower than E_2. These peaks depend on molecular ground state properties and the probe laser only. For this reason they can be observed also for negative delays $\tau < 0$.

The population of the π_z^* state increases with the delay for $\tau > 0$. At about the same τ for which E_1 becomes visible, the peak at $E_3 = \omega_{\mathcal{P}} + \omega_p - I_P = 1.679$ Ha begins to emerge. This peak corresponds to electrons ejected into the continuum from the π_z^* state, which is transiently occupied via the pump pulse.

To further analyse the results, in figure 3 we plot a cut of the TRPES at $\tau_f = 7.26$ fs, after the pump has been switched off. In the figure we introduce new peak labels in addition to E_1, E_2, E_3, which have been previously discussed. These labels identify the contribution to each peak from the ground state KS orbitals of ethylene shown in figure 1.
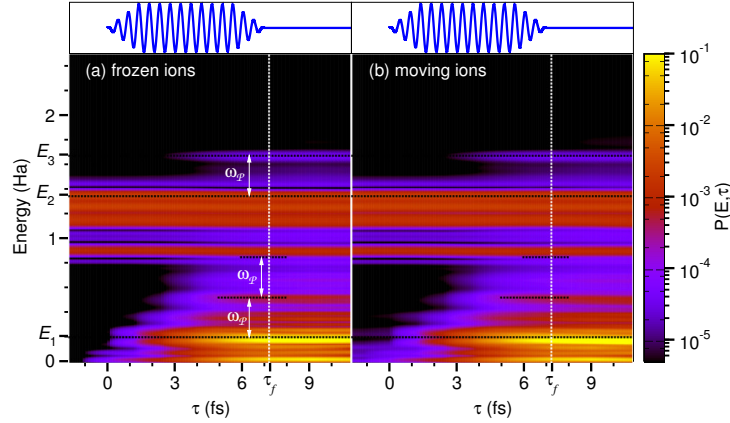
Figure 2. TRPES $P(E, \tau)$ of ethylene as a function of the photoelectron's kinetic energy in Ha and the pump-probe time delay τ in fs with frozen (a), or moving (b) nuclei. Nuclear motion is modelled with an initial temperature of 300 K. Pump (blue) and probe (violet) pulses are polarized with laser parameters as described in figure 1. The pump is depicted in the upper panels of (a) and (b) as a function of τ. Here $E_1 = 2\omega_P - I_p$, $E_2 = \omega_p - I_p$, $E_3 = \omega_P + \omega_p - I_P$. The energies $E_1, E_1 + \omega_P, E_1 + 2\omega_P, E_2, E_3$ ($\cdots\cdots$ black) and the time delay τ_f ($\cdots\cdots$ white) are shown to guide the eye. White arrows correspond to the pump's energy ω_P.
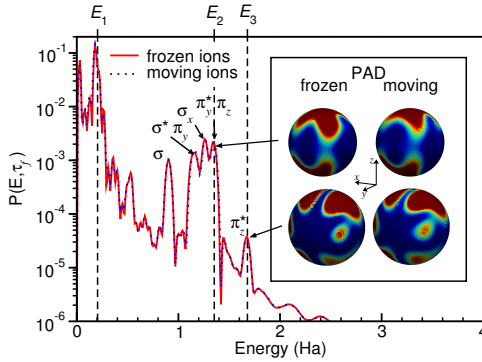

Figure 3. Photoemission spectra of ethylene versus the photoelectron's kinetic energy in Ha for a probe applied at the end of the pump ($\tau_f = 7.26$ fs as shown in figure 2) $P(E, \tau_f)$. The nuclei are either frozen (red), or their motion is classically modelled at an initial temperature of 300 K (blue). Peaks at E_1, E_2 and E_3 correspond to the energy transitions described in figure 2, while those labelled σ, σ^*, π_y, σ_x and π_y^* correspond to direct excitations by the probe from the respective orbitals depicted in figure 1. PADs for ethylene at the energies E_2 and E_3 when the pump has ended τ_f for frozen and moving nuclei are shown in the inset.

Supplementary information regarding the nature of PES peaks can be obtained from the PADs. For electrons ejected from orbitals with π-symmetry, the momentum resolved photoelectron probability is approximately $P(\mathbf{p}) \sim |\mathbf{A} \cdot \mathbf{p}|^2 |\tilde{\varphi}(\mathbf{p})|^2$, where $\tilde{\varphi}(\mathbf{p})$ is the Fourier transform of the initial orbital [57] and $\mathbf{A}(t) = \int_0^t d\tau \mathbf{E}(\tau)$ is the vector potential in the velocity gauge. PADs for angles close to the laser polarization direction, where the polarization factor $|\mathbf{A} \cdot \mathbf{p}|$ is close to unity, reflect the nodal symmetry of the orbital from which the electron has been ejected.

The inset of figure 3 shows how the frozen and moving nuclei's PADs correlate with the originating orbital symmetry. Photoelectrons emerging with kinetic energy E_2 are ejected from almost degenerate π_y^* and π_z orbitals. The PADs associated with E_2 coherently display a symmetry compatible with the superposition of these orbitals. On the other hand, the PADs for E_3 present a nodal structure clearly linked to a π_z^* orbital symmetry.

As shown in figure 2(b), the effect of nuclear motion on the electronic TRPES is negligible. Further, the PAD is minimally changed by the effect of moving the nuclei as shown in the inset of figure 3.

On the one hand, the occupation of the antibonding π_z^* orbital is not significant throughout the simulation. There are two main reasons for this outcome. The first one traces back to known problems in describing resonant state population with adiabatic TDDFT. This is related to inaccuracies in the time dependence of the xc-kernel [58]. The second reason is the depopulation of the π_z^* orbital through the direct ionization channel observed at E_1.
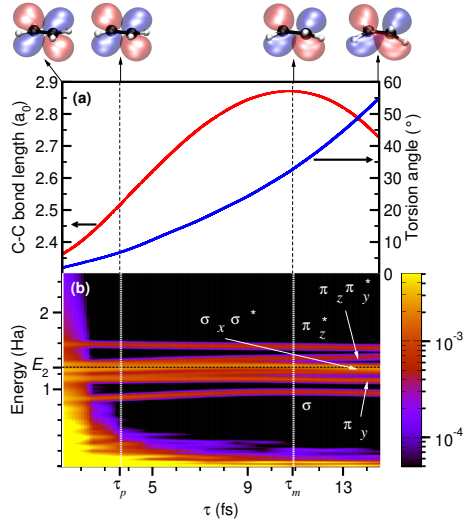
Figure 4. (a) Ethylene carbon-carbon bond length in a_0 (red) and torsion angle in ° (blue) versus the probe time delay τ in fs from an artificial $\pi_z \rightarrow \pi_z^*$ excited initial state. The nuclei's motion is classically modelled starting from 300 K and the ground state. The black vertical lines are the times at which the C–C bond length reaches its maximum $\tau_m = 10.8$ fs and a previous time $\tau_p = 3.6$ fs for comparison. The molecular structure and π_z^* orbital at the start, τ_p, τ_m and end of the simulation are shown above. (b) Probe TRPES $P(E, \tau)$ for all the labelled orbitals of ethylene in figure 1, as a function of the photoelectron's kinetic energy in Ha and the probe time delay τ in fs (see figure 1 for details of the probe) starting from the ground state. The nuclei's motion is classically modelled with an initial temperature of 300 K. The black ······ vertical lines are the times at which the C–C bond length reaches its maximum $\tau_m = 10.8$ fs and a previous time $\tau_p = 3.6$ fs for comparison.

On the other hand, changes of the TRPES due to nuclear motion are also small because they are calculated over a large energy range (3Ha). This is done to include the evolution of all the ethylene orbitals shown in figure 1.

As a result, the molecular geometry is minimally modified during the action of the pump pulse, with a maximum change in the C–C bond-length of less than 0.033 a_0. For the laser parameters depicted in figure 1, the photoelectron properties of the molecule are largely unaffected by the coupling with nuclear degrees of freedom. Although the bandwidth of the probe (~ 0.05 Ha) can resolve electronic transitions, it is too wide to resolve vibrational and thermal effects. As a result, effects due to the initial temperature do not appear in the TRPES [59].
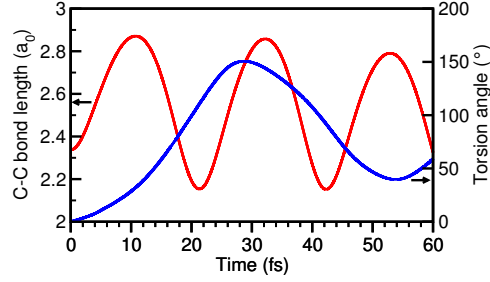

Figure 5. Ethylene carbon-carbon bond length in a_0 (red) and torsion angle in ° (blue) as a function of time in fs, with the nuclei's motion classically modelled starting from 300 K and a molecular excited state created by artificially promoting one electron from the KS HOMO to the LUMO.

A stronger nuclear response can be stimulated by propagating a fully occupied electronic excited state. In the previous case, the pump laser was in charge of populating an excited state, which was subsequently observed during its construction, by means of a delayed probe pulse. We now investigate the effect of the coupling between nuclear and electronic degrees of freedom while keeping an excited state fully populated.

To this end, we artificially promote one electron from the highest occupied KS molecular orbital (HOMO) to the first unoccupied one (LUMO), and propagate keeping this configuration. The KS LUMO with π^* symmetry is of antibonding nature. We thus expect its occupation to have sizeable effects on the nuclei's motion, especially on the C–C bond. We employ the same probe pulse shown in figure 1, while the pump pulse has been omitted. Here, the time delay is measured as the difference from the center of the probe to the starting point of the time evolution.

Changes in the bond length and the torsion of the molecule induced by the initial electronic excitation are shown on the left and right hand side of figure 4 (a), respectively. The same is shown in figure 5 for a longer time propagation. The C–C bond length displays an oscillatory behaviour. It initially increases up to 0.53 a_0 at $\tau_m = 10.8$ fs over its initial ground state equilibrium position, and then oscillates in time.

The molecule undergoes a twist along the C–C axis reaching a maximum torsion of 150.6°. This behavior is at the core of cis-trans isomerization processes happening in many photochemical reactions [60]. The vibrational stretching frequency along the C–C bond ($\omega_{CC} = 7.14 \times 10^{-3}$ Ha) and the torsional distortion
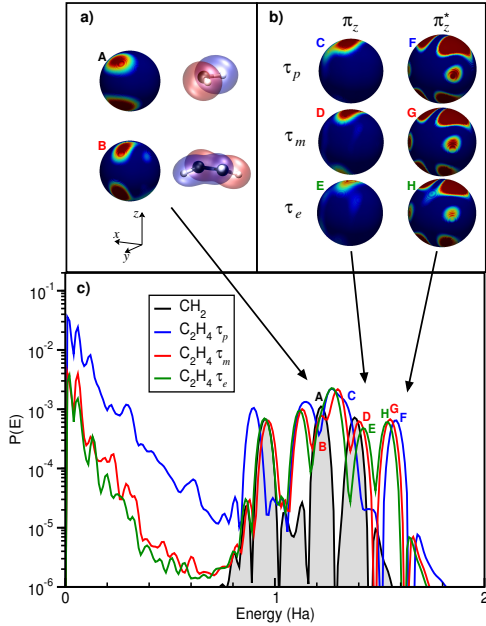
Figure 6. (a) PADs and π_y orbitals for methylene (A) and ethylene (B). (b) Ethylene PADs for π_z/π_z^* orbitals at τ_p, τ_m and τ_e. (c) PES for a probe applied to the methylene molecule and to the ethylene molecule for the time at which the C–C bond length reaches its maximum $\tau_m = 10.8$ fs, an earlier time $\tau_p = 3.6 < \tau_m$ fs and at the end of the simulation $\tau_e = 14.5$ fs. The PAD for the peaks labelled in the PES for both ethylene and methylene are shown in (a) and (b).

($\omega_{torsion} = 2.82 \times 10^{-3}$ Ha) are in qualitative agreement with the experimental data ($\omega_{CC} = 7.39 \times 10^{-3}$ Ha and $\omega_{torsion} = 4.67 \times 10^{-3}$ Ha) [60].

These modifications of the molecule's geometry are reflected in the TRPES shown in figure 4 (b). For time delays $\tau \leq \tau_p$ we have five initial peaks in the TRPES, as we had in the pump-probe case (see figures 2 and 3). However, now the initial spectrum changes in time, as the peaks shift in position and new ones emerge close to the maximum elongation of the C–C bond.

The lowest energy peak oscillates in energy in phase with the C–C bond length. This peak is consistent with all-bonding σ orbital electrons (see figure 1), and is therefore sensitive to the molecule's bond-length and relatively insensitive to its torsion angle.

The following peak in energy splits into two new peaks. The peak that shifts in energy, corresponds to the π_y state, whereas the one that does not, to the σ^* state. The π_y state energy shift is due to the fact that it connects hydrogens bound to dif-

ferent carbon atoms, and is therefore sensitive to the molecule's torsion and the C–C bond length.

The intermediate peak in energy corresponds to the σ_x state, which does not shift in energy, as it is only weakly affected by the molecule's bond stretching.

The second to last peak in energy corresponds to the π_y^* and π_z states. The former shifts towards lower energies because it does not connect hydrogens bound to different carbon atoms, and the latter depletes probability along the nodal plane, shifting towards higher energies.

The highest and last peak in energy is consistent with the π_z^* and it shifts towards lower energies because it builds probability along the nodal plane.

The π_z^* and π_z orbitals become degenerate when a torsion angle of 90° is reached. The LUMO π_z^* orbital evolution is shown on top of figure 4.

In order to support this analysis, in figure 6 (c) we present selected cuts of the TRPES at the specific time delays $\tau_p = 3.6$ fs, $\tau_m = 10.8$ fs and $\tau_e = 14.5$ fs. The time evolution of each photoelectron peak, can here be monitored identifying each peak with its PAD *fingerprint* in figures 6 (a) and (b). The peaks labelled **F**, **G**, **H**, which shift towards lower energies as time evolves, belong to the same state according to the PADs. This state can easily be associated to a π_z^* orbital due to its nodal structure. Similarly, the peaks **C**, **D**, **E**, which shift towards higher energies as time evolves, all originate from the same π_z orbital.

In comparison to the HOMO E_2 PADs we observed in the pump-probe case of figure 3, the π_z character is here more defined. This is because the occupation of the KS LUMO state is lifting the π_y^*, π_z degeneracy that we had previously. When the C–C elongation is at its maximum value at τ_m, a new peak emerges at $E_{\mathbf{B}} = 1.22$ Ha, which disappears at τ_e.

In order to understand where this extra peak comes from, we have obtained the photoelectron spectrum of methylene with the same probe pulse used for ethylene as shown filled in figure 6 (c). The PADs and orbitals of the peaks labelled **B** (belonging to ethylene) and **A** (belonging to methylene) in figure 6 (a) display a π_y symmetry. We can therefore conclude, that this extra peak is related to the π_y ethylene state which becomes less stable as the C–C bond length increases.

The first main peak corresponds to a σ state, which increases in energy until τ_m and then decreases again until τ_e as shown in the PES in figure 6 (c). The second main peak shifts towards

lower energies as time evolves. This corresponds to the σ^* and π_y states, which separate in energy at τ_m, as explained above.

4. Conclusions

In this paper we investigated the impact of nuclear degrees of freedom in TRPES and TRPAD for the test case of the ethylene molecule.

We first studied the case where a pump laser resonantly excites a bound state which is subsequently probed by a time delayed pulse with attosecond time scale resolution. The applied pump does not induce a sufficient occupation of the antibonding π_z^* orbital for changes in the nuclear positions to be resolved by the probe. The photoelectron spectrum is therefore minimally modified on the energy scales considered.

In order to induce detectable nuclear effects we studied the time evolution of a molecular excited state created by artificially promoting one electron from the KS HOMO to the LUMO. This promotion has proven to be sufficient to excite vibrational C–C bond and torsional modes. TRPES in this case has shown major changes that can be understood in terms of PADs and orbital deformations associated to nuclear rearrangements.

This work is an initial step towards a scalable TDDFT scheme for ab-initio simulation of time resolved photoemission processes coupled with nuclear motion. Further effort will be spent in the future on the road to the inclusion of nuclear effects beyond Ehrenfest.

Acknowledgments

References

[1] Haight R 1995 *Surf. Sci. Rep.* **21** 275
[2] Cyr D R and Hayden C C 1996 *J. Chem. Phys.* **104**
[3] Greenblatt B J, Zanni M T and Neumark D M 1997 *Science* **276** 1675
[4] Petek H and Ogawa S 1997 *Prog. Surf. Sci.* **56** 239
[5] Blanchet V, Zgierski M Z, Seideman T and Stolow A 1999 *Nature (London)* **401** 52
[6] Lehr L, Zanni M T, Frischkorn C, Weinkauf R and Neumark D M 1999 *Science* **284** 635
[7] Neumark D M 2001 *Annu. Rev. Phys. Chem.* **52** 255
[8] Reid K L 2003 *Annu. Rev. Phys. Chem.* **54** 397
[9] Stolow A 2003 *Annu. Rev. Phys. Chem.* **54** 89
[10] Pazourek R, Feist J, Nagele S and Burgdörfer J 2012 *Phys. Rev. Lett.* **108** 163001
[11] Smallwood C L, Hinton J P, Jozwiak C, Zhang W, Koralek J D, Eisaki H, Lee D H, Orenstein J and Lanzara A 2012 *Science* **336** 1137–1139
[12] Graf J, Jozwiak C, Smallwood C L, Eisaki H, Kaindl R A, Lee D H and Lanzara A 2011 *Nat Phys.* **7** 805–809
[13] Zewail A 2000 *J. Phys. Chem. A* **104** 5660
[14] Foggi P, Bussotti L and V R Neuwahl F 2001 *International Journal of Photoenergy* 103–109
[15] Brabec T and Krausz F 2000 *Rev. Mod. Phys.* **72** 545–591
[16] Plaja L, Torres R and Zaïr A (eds) 2013 *Attosecond Physics* (*Springer Series in Optical Sciences* vol 177) (Berlin, Heidelberg: Springer Berlin Heidelberg)
[17] Sansone G, Kelkensberg F, Perez-Torres J F, Morales F, Kling M F, Siu W, Ghafur O, Johnsson P, Swoboda M, Benedetti E, Ferrari F, Lepine F, Sanz-Vicario J L, Zherebtsov S, Znakovskaya I, LHuillier A, Ivanov M, Nisoli M, Martin F and Vrakking M J J 2010 *Nature* **465** 763–766
[18] Siu W, Kelkensberg F, Gademann G, Rouzee A, Johnsson P, Dowek D, Lucchini M, Calegari F, De Giovannini U, Rubio A, Lucchese R, Kono H, Lepine F and Vrakking M J 2011 *Phys. Rev. A* **84**
[19] Zhou X, Ranitovic P, Hogle C W, Eland J H D, Kapteyn H C and Murnane M M 2012 *Nat Phys.* **8** 232–237
[20] Wu G, Hockett P and Stolow A 2011 *Phys. Chem. Chem. Phys.* **13** 18447–18467
[21] Bisgaard C Z, Clarkin O J, Wu G, Lee A M D, Gessner O, Hayden C C and Stolow A 2009 *Science* **323** 1464–1468
[22] Gessner O, Lee A M D, Shaffer J P, Reisler H, Levchenko S V, Krylov A I, Underwood J G, Shi H, East A L L, Wardlaw D M, Chrysostom E t H, Hayden C C and Stolow A 2006 *Science* **311** 219–222
[23] Freericks J K, Krishnamurthy H R and Pruschke T 2009 *Phys. Rev. Lett.* **102** 136401–136405
[24] Feist J, Nagele S, Pazourek R, Persson E, Schneider B, Collins L and Burgdörfer J 2008 *Phys. Rev. A* **77** 043420
[25] Ishikawa K L and Ueda K 2012 *Phys. Rev. Lett.* **108** 033003
[26] Argenti L, Pazourek R, Feist J, Nagele S, Liertzer

M, Persson E, Burgdörfer J and Lindroth E 2013 *Phys. Rev. A* **87** 053405

[27] Schafer K and Kulander K 1990 *Physical Review A* **42** 5794–5797

[28] Boguslavskiy A E, Mikosch J, Gijsbertsen A, Spanner M, Patchkovskii S, Gador N, Vrakking M J J and Stolow A 2012 *Science* **335** 1336–1340

[29] Lucchese R, Raseev G and McKoy V 1982 *Phys. Rev. A* **25** 2572–2587

[30] Arasaki Y, Takatsuka K, Wang K and McKoy V 2010 *J. Chem. Phys.* **132** 124307

[31] Suzuki Y, Stener M and Seideman T 2003 *J. Chem. Phys.* **118** 4432

[32] Tao H, Allison T K, Wright T W, Stooke A M, Khurmi C, van Tilborg J, Liu Y, Falcone R W, Belkacem A, and Martinez T J 2011 *J. Chem. Phys.* **134** 244306

[33] Tao H, Levine B G and Martinez T J 2009 *J. Phys. Chem. A* **113** 13656

[34] Stanzel J, Burmeister F, Neeb M, Eberhardt W, Mitric R, Burgeland C and Bonacic-Koutecky V 2007 *J. Chem. Phys.* **127** 164312

[35] Mignolet B, Levine R D and Remacle F 2014 *Phys. Rev. A* **89** 021403

[36] Ullrich C A 2012 *Time-Dependent Density-Functional Theory: Concepts and Applications* (Oxford University Press)

[37] Marques M, Maitra N, Nogueira F, Gross E and Rubio A (eds) 2012 *Fundamentals of Time-Dependent Density Functional Theory* (*Lecture Notes in Physics* vol 837) (Berlin: Springer)

[38] Pohl A, Reinhard P and Suraud E 2000 *Phys. Rev. Lett.* **84** 5090

[39] Pohl A, Reinhard P and Suraud E 2004 *Phys. Rev. A* **70** 023202

[40] Giovannini U D, Varsano D, Marques M A L, Appel H, Gross E K U and Rubio A 2012 *Physical Review A* **85** 062515

[41] Giovannini U D, Brunetto G, Castro A, Walkenhorst J and Rubio A 2013 *Chemphyschem* **14** 1363–1376

[42] Alonso J, Andrade X, Echenique P, Falceto F, Prada-Gracia D, Rubio A and Rubio A 2008 *Phys. Rev. Lett.* **101** 096403

[43] Andrade X, Castro A, Zueco D, Alonso J L, Echenique P, Falceto F and Rubio A 2009 *J. Chem. Theory Comput.* **5** 728–742

[44] Runge E and Gross E K U 1984 *Phys. Rev. Lett.* **52** 997

[45] Kohn W and Sham L J 1965 *Physical Review* **140** A4: A1133

[46] Perdew J P and Zunger A 1981 *Phys Rev B* **23** 5048–5079

[47] Legrand C, Suraud E and Reinhard P G 2002 *Journal of Physics B: Atomic, Molecular and Optical Physics* **35** 1115–1128

[48] Zhi-Ping W, Jing W and Feng-Shou Z 2010 *Chinese Phys. Lett.* **27** 013101

[49] Wang Z P, Dinh P M, Reinhard P G, Suraud E and Zhang F S 2011 *Int. J. Quantum Chem.* 480–486

[50] Troullier N and Martins J L 1991 *Phys. Rev. B* **43** 1993

[51] Castro A, Marques M, Appel H, Oliveira M, Rozzi C, Andrade X, Lorenzen F, Gross E and Rubio A 2006 *Phys. stat. sol* **243** 2465–2488

[52] Andrade X, Alberdi-Rodriguez J, Strubbe D A, Oliveira M T, Nogueira F, Castro A, Muguerza J, Arruabarrena A, Louie S, Aspuru-Guzik A, Rubio A and Marques M 2012 *J. Phys.: Condens. Matter* **24** 12

[53] Marques M, Castro A, Bertsch G and Rubio A 2003 *Computer Physics Communications* **151** 60–78

[54] Castro A, Marques M A L and Rubio A 2004 *J Chem. Phys.* **121** 3425–3433

[55] Craig N C, Groner P and McKean D C 2006 *J. Phys. Chem. A* **110** 7461–7469

[56] Turner D W, Baker C, Baker A D, and Brundle C R (eds) 1970 *Molecular Photoelectron Spectroscopy* (London: Wiley)

[57] Puschnig P, Berkebile S, Fleming A J, Koller G, Emtsev K, Seyller T, Riley J D, Ambrosch-Draxl C, Netzer F P and Ramsey M G 2009 *Science* **326** 702–706

[58] Fuks J I, Elliott P, Rubio A and Maitra N T 2013 *J. Phys. Chem. Lett.* **4** 735–739

[59] Wollenhaupt M, Engel V and Baumert T 2005 *Annu. Rev. Phys. Chem.* **56** 25–56

[60] Kunert T, Grossmann F and Schmidt R 2005 *Phys. Rev. A* **72** 023422